the same energy.

In conclusion, the light-scattering cross section depends on the polarization of the incoming and outgoing photons as well as on the wave-vector and frequency transfer to the system. It is possible, for anisotropic semiconductors, to change the strength of the effective electron-photon coupling to the different valleys by changing the polarization directions. It is also possible to change the mass ratio of the "light" and "heavy" electrons by changing the direction of q. We note that typical mass ratios are about 1 : 3, and the dynamic susceptibilities of both the light- and heavy-mass electrons must be assumed. Thus detailed calculations would be necessary to compare theory with experimentally observed spectra.

It is also noteworthy that, as seen from our numerical computations, a contribution from ion-acoustic waves appears (see Fig. 1, curve 2 and Fig. 2, curve 2), although the mass ratio is small. In our case we find this effect to be due to larger coupling of the photon to the heavy rather than the light electron. On the other hand, when the photon strongly couples to the light electrons one observes a deep dip (see Fig. 1, curve 3 and Fig. 2, curve 4) at the ion-acoustic frequency.

*Research sponsored by the U. S. Air Force Office of Scientific Research Air Force System Command, U. S. Air Force, under AFOSR Grant No. 71-1978.

[1]A. Mooradian and G. B. Wright, Phys. Rev. Letters 16, 999 (1966).

[2]D. C. Hamilton and A. L. McWhorter, in *Light Scattering Spectra in Solids*, edited by G. B. Wright (Springer, New York, 1969), p. 309.

[3]S. S. Jha, Phys. Rev. 182, 815 (1969); 179, 764 (1969).

[4]P. M. Platzman, Phys. Rev. 139, A379 (1965).

[5]A. L. McWhorter, in *Physics of Quantum Electronics*, edited by P. L. Kelley, B. Lax, and P. E. Tannanwald (McGraw-Hill, New York, 1966), pp. 111–118.

[6]N. Tzoar and E-Ni. Foo, in *Proceedings of the Second International Conference on Light Scattering in Solids* (Flammarion, Paris, 1971). In this paper only contributions to the cross section from CDF are presented.

[7]P. A. Wolff, Phys. Rev. 171, 436 (1968).

[8]A. J. Glick and R. A. Ferrell, Ann. Phys. (N.Y.) 11, 359 (1960).

PHYSICAL REVIEW B VOLUME 6, NUMBER 12 15 DECEMBER 1972

Impurity Ionization in n-Type Germanium

J. F. Palmier

Departement P.M.T., Centre National D'Etudes des Telecommunications, 22-Lannion, France

(Received 11 February 1972)

Impurity ionization in semiconductors at low temperatures is the excitation of trapped electrons on shallow levels to the conduction band by the impact of electrons heated by a sufficient electric field. The hot-electron mobility and the impact-ionization cross section are studied separately, by the microwave mobility of the avalanche plasma (during short current pulses) and by the transient response of high-impedance samples, respectively. The basis of any interpretation is the correct calculation of some hot-electron distribution functions. During the discharge regime (steady electric field, current increasing by orders of magnitude), the mobility remains nearly constant. For purer samples, the values of the mobility agree within 30% with the hypothesis of pure emission of acoustical phonons. For less pure samples, the mobility decreases with the donor concentration and neutral impurity scattering dominates ionized impurity scattering. The saturation regime is also investigated for a pure sample where some heating of phonons occurs. A precise calculation of the coupled system of Boltzmann equations indicates a mean free path of phonons greater than the transverse width of the sample. Several impact-ionization cross-section laws are tested to compare the results of the transient-pulse analysis with the theoretical ionization rate, which is an average of that cross section weighted by the distribution function. Mobility and ionization rate measurements indirectly give the Auger recombination parameter, which is compared with previous data for much lower energies and with the cascade capture theory.

INTRODUCTION

Impact ionization of shallow impurities in semiconductors at low temperatures is now a familiar phenomenon and has been studied both theoretically and experimentally[1–6] during the past ten years. The values obtained for the critical field E_c have been extensively discussed in terms of hot-electron distribution functions, impact-ionization cross sections, and recombination probabilities. The

threshold field E_c is usually determined by a comparison between the impact-ionization rate and the giant-traps recombination process.[7–9] However, such a discussion can lead to only qualitative results because of the large number of parameters entering the problem. In the present work, the hot-electron problem and the impact-ionization problem have been separated. Independent measurements of the hot-electron mobility during breakdown and of the impact-ionization rate are reported and compared, both during the discharge regime ($E = E_c$) and in the saturation range ($E > E_c$). Simple interpretations can only be derived when the hot-electron distribution function does not depend on the impact-ionization cross section, i.e., when the mean power lost in ionization collisions is much smaller than the mean power lost by electron-phonon processes. This condition is not difficult to realize with a moderately doped sample of n-Ge. Mobility measurements during breakdown are difficult to achieve by the usual techniques, since transverse inhomogeneities of the hot-electron plasma occur at the lowest temperatures and a transverse magnetic field strongly modifies the distribution function.[10,11] We have therefore used a suitable microwave diagnostic technique to give a direct measurement of the mobility through some average of the momentum relaxation time τ_1. Thus we can define a microwave mobility μ_m, which is related to the drift mobility μ by a numerical factor arising from a suitable average over the distribution function $f(\vec{p})$. The impact-ionization rate $A_I = \langle \sigma_i(\epsilon) v \rangle$, where $\sigma_i(\epsilon)$ is the impact-ionization cross section and ϵ and v the energy and velocity of the primary electron, is directly measured by a transient pulse technique at $E > E_c$ by using a method that avoids any heating of the sample and the nonequilibrium distribution function for phonons.[12,13] Then, the values obtained for μ, the mean electron density n, and the impact-ionization rate A_I lead to the inverse process parameter B_I (Auger recombination rate) through the balance equation relating B_I, B_T, A_I, n, ..., and the impurity concentrations.

The present paper is divided into three sections. Section I is devoted to a complete discussion of the microwave diagnostic technique within a hot-electron avalanche plasma, and to the question of the microwave mobility, i.e., to the usefulness and accuracy of the method. In Sec. II, the hot-electron problem for n-type Ge at low temperatures is discussed within the limits where it is not dependent on the impact-ionization problem. Hot electrons are mainly coupled to acoustical phonons and three cases are discussed: (i) The phonon density N_q can be neglected compared with 1 in the transition probabilities, i.e., zero-point or pure-emission limit, (ii) $N_q = \bar{N}_q$, the equilibrium value, and (iii) N_q is given by a transport equation coupled to the hot-electron distribution function. The last case is developed from a new point of view and compared with the previous theory of Conwell[12] since the relevant electron density in the present experiments is too low to assume the validity of a pure Maxwell distribution for $f(\vec{p})$. A numerical method is given for the solution of the coupled Boltzmann equations. In Sec. III, a comparison between the experimental and theoretical values of $A_I(E)$ at $E > E_c$ is considered for As and Sb centers, involving the consideration of the mobility results. It also includes the measurement of B_I, values of which are compared with the previous results of Koenig *et al.*[1] for equilibrium electrons. The ratio of the two values of B_I gives rise to some conclusion on the Auger recombination process. In the final conclusion the contribution of the present work is outlined and compared with previous estimations and theories.

I. EXPERIMENTAL PROCEDURE AND THE MICROWAVE DIAGNOSTIC

Table I sums up the general properties of the different Ge specimens used in the present experiments. N_D and N_A are, respectively, the donor and acceptor concentrations and E_c is the breakdown critical field. All the samples were cut to a long parallelepiped shape ($12 \times 1 \times 1$ mm^3), except sample (a), which was reduced to ($7 \times 0.4 \times 0.4$ mm^3) to allow for a better microwave diagnostic in the saturation range (which requires a small transverse size to give reliable data when $E > E_c$). Then the samples were etched and Ohmic contacts with platinum wires were soldered at its ends. The samples could be introduced into the center hole of a microwave cavity as shown in Fig. 1. Two coaxial lines were soldered to the platinum wires. The electronic apparatus is shown schematically in Fig. 2.

Figure (3) represents different transmission curves of the cavity measured during current pulses in sample (a). One can see the strong per-

TABLE I. General properties of the n-Ge samples used in the present experiments. Samples (b) and (d) are, respectively, samples (1a) and (2a) of Ref. 14.

Ref. Sample	$N_D - N_A$ (cm^{-3})	N_A (cm^{-3})	E_c (V cm^{-1})	Impurity
(a)	6×10^{13}	$< 10^{13}$	6.1	Sb
(b)	1.5×10^{14}	5×10^{13}	7.5	As
(c)	2×10^{14}	5×10^{13}	9	As
(d)	3×10^{14}	10^{14}	15	As
(e)	4×10^{14}	$< 10^{14}$	10	Sb
(f)	5×10^{15}	...	55	As
(g)	2×10^{16}	...	65	As

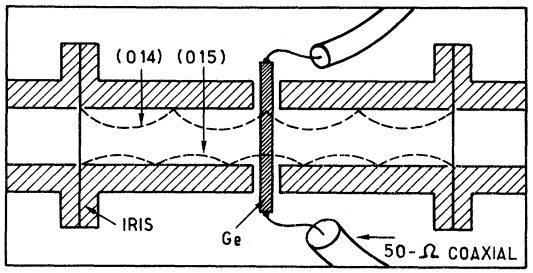

FIG. 1. Schematic drawing of the 8-mm wavelength cavity. The electric field charts of TE014 and TE015 modes show clearly how they behave differently with respect to the perturbation of the avalanche plasma. Mode (014) is particularly interesting for the saturation analysis.

turbation of the resonance curves with the number of carriers in the sample. The cavity presented in Fig. 1 operates in the 8-mm-wavelength range and can be tuned to the TE014 (32 GHz) or TE015 (35.5 GHz) modes. The first mode is weakly perturbed by the plasma since it provides a very weak rf electric field probe within the sample, which is well suited for high-density measurements ($E > E_c$). However, the second mode has a maximum of the

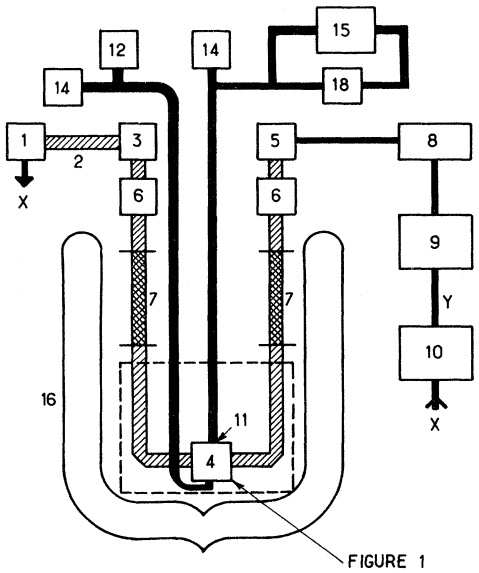

FIG. 2. Electronic apparatus. (1) B.W.O. frequency swept from 26 to 40 GHz; (2) waveguide, internal cross section 7.12×3.56 mm^2; (3) attenuator; (4) cavity (see Fig. 1); (5) detection diode; (6) ferrite isolators; (7) stainless-steel waveguide sections (25 cm); (8) video preamplifier ($\times 100$); (9) pulse integrator (Boxcar from P.A.R.); (10) xy recorder; (11) coaxial line; (12) pulse generator 0–70 V, risetime < 5 nsec, rate 10 Hz; (14) 50 Ω; (15) two channels sampling oscilloscope; (16) helium Dewar and shielding; (18) R-C differentiator circuit.

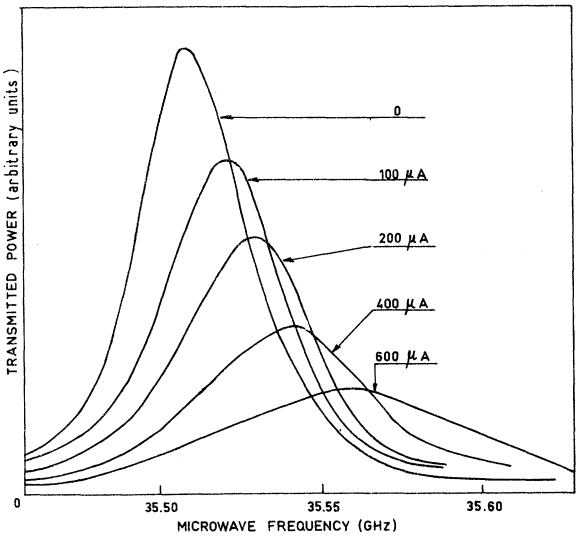

FIG. 3. Power transmitted by the cavity versus the microwave frequency for several values of the current I [sample (a), mode (015)].

rf electric field probe in the sample and gives the diagnostic for moderate current values. For the lowest currents, it is better to use a lower frequency range of the apparatus, with exactly the same principle of measurement. In an earlier paper[14] the results obtained at 4 GHz were presented. From the transmission curves in Fig. 3 one can measure the resonant-frequency shifts ΔF and the quality factor variations $\Delta(1/Q)$, the origin of the variations being the zero-current values, since the moderately doped samples are quasipure dielectrics at microwave frequencies (see Fig. 4). A well-known perturbation theory gives[14–17]

$$\Delta F/F = -\tfrac{1}{2}\varphi\,\mathrm{Im}(\hat{\sigma})\,, \qquad \Delta(1/Q) = \varphi\,\mathrm{Re}(\hat{\sigma})\,, \tag{1}$$

where φ is a shape factor and $\mathrm{Im}(\hat{\sigma})$ and $\mathrm{Re}(\hat{\sigma})$ are the imaginary and real parts of the microwave conductivity $\hat{\sigma}$. The validity of Eqs. (1) is completely discussed for a gaseous plasma in Ref. 18, where the result of the exact solution of Maxwell equations in a similar case is compared with Eqs. (1). For a collisionless plasma ($\omega\tau_1 \gg 1$), a critical density can be defined by $\omega^2 = \omega_p^2 = ne^2/m^*K_R$, where K_R is the lattice permittivity and m^* a suitable effective mass. Above the critical density corresponding to $\omega = \omega_0$, Eqs. (1) remain valid only if the geometrical perturbation remains weak. Thus a thin sample diameter or a weakly perturbing mode such as TE014 is implied in the present case (Fig. 1). The present method of measurement of the transient microwave conductivity is limited in three factors.

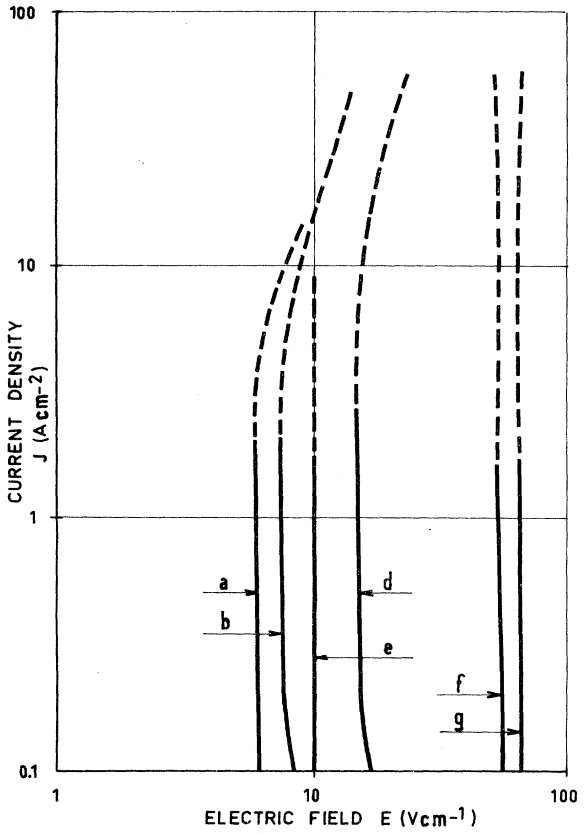

FIG. 4. Classical $j(E)$ data. The current density j is deduced from the total current I.

(i) There is a minimum of current in the sample, under which it is very difficult to stabilize the plasma and to obtain meaningful measurements of ΔF and $F_0\ \Delta(1/Q)$, since the whole system becomes unstable. The origin of the instability probably lies in a phonon-induced recombination mechanism, which is beyond the scope of the present paper.[15,16]

(ii) There is also a maximum of current for the method's validity, i.e., for a correct interpretation of Eqs. (1). With a suitable correction due to K_R and m^*, the maximum density is $\sim 10^{14}$ cm^{-3} as a limit for a 0.5-mm-thick bar in the microwave cavity at $F_0 = 32$ GHz. The critical density given by $\omega = \omega_p$ would be only 2×10^{13} cm^{-3}.

(iii) The rise time of the apparatus is basically limited by the microwave cavity itself: $Q/\pi F_0 \sim 10$ nsec at $F_0 = 35$ GHz with $Q \sim 700$. However, technical difficulties arise from the detector, which cannot have a high sensitivity and a fast response simultaneously. The whole response time of the system is only ~ 0.1 μsec. The usefulness of Eqs. (1) derives from the numerical factor Z,

$$Z = \frac{\Delta F}{F\Delta(1/Q)} = -\frac{1}{2}\frac{\mathrm{Im}(\hat{\sigma})}{\mathrm{Re}(\hat{\sigma})}\ , \tag{2}$$

which is independent of the shape factor φ. Even if conduction occurs in a thin filament, it is possible to give some information on the conduction process in that filament. What information is given by Z? The complete calculation of $\hat{\sigma}$ from the hot-electron distribution function is possible, at least in the case $\omega\tau_1 \gg 1$.

The well-known theory of microwave conductivity is based upon first and second momenta of the Boltzmann equation.[19] That theory leads to a modulation of the mean velocity $\langle v\rangle$ through the energy relaxation time τ_2 and the momentum relaxation time τ_1. We only add the impurity scattering to the previous theory, as

$$\tau_1^{-1} = \tau_a^{-1} + \tau_i^{-1} + \tau_n^{-1}\ , \tag{3}$$

where τ_a, τ_i, τ_n are, respectively, the relaxation times, limited by acoustical phonons, ionized impurities, and neutral impurities.

Then the microwave velocity is

$$\hat{v} = \mu\hat{E}\ \frac{n_1 + n_2 - N + i\omega\tau_2}{N + (1+i\omega\tau_1)(n_1+n_2+i\omega\tau_2)}\ , \tag{4}$$

with

$$N = \tau_1(n_1/\tau_a - 1.5/\tau_i)\ . \tag{5}$$

In Eq. (4) we assume that

$$\tau_2 \sim \langle\epsilon\rangle^{-n_2}\ ,\quad \tau_a \sim \langle\epsilon\rangle^{-n_1}\ ,\quad \tau_i \sim \langle\epsilon\rangle^{1.5}\ . \tag{6}$$

In addition to a modulation of the drift velocity, the carrier density may be modulated because of the impact ionization.

Price[20] has given a semiphenomenological derivation of the density evolution by the following equation:

$$\frac{dn}{dt} = (N_D - N_A - n)(A_T + nA_I) - n(N_A + n)(B_T + nB_I)\ , \tag{7}$$

where A_T, A_I, B_T, and B_I are, respectively, the thermal generation, impact-ionization, thermal recombination, and Auger recombination rates. By the same procedure that gives $\hat{v}$, one readily obtains

$$\hat{n} = n\hat{E}\ \frac{A_I'(N_D - N_A - n) - B_T'(N_A + n) - B_I'n(N_A + n)}{A_T + i\omega + n(B_T + A_I) + 2nB_I(N_A + n)}\ , \tag{8}$$

where A_I', B_T', and B_I' are the derivatives of the kinetic parameters with respect to E. Then the microwave conductivity is given by $\hat{\sigma} = e(n\hat{v} + \hat{n}v)/\hat{E}$ and the general expression of Z is awkward. Drastic simplifications can be made in the peculiar case of n-Ge at 4 °K with the following conditions: (a) $\tau_2 \gg \tau_1$, which is often realized in practice; (b) $(\omega\tau_2)^2 \gg 1$, which implies that $F_0 > 1$ GHz; (c) $A_I(N_D - N_A)$, B_TN_A, $B_InN_A \ll \omega$, which is easily realized for a moderately doped sample as soon as $\omega\tau_2 > 1$. If these three conditions are realized

simultaneously, the factor Z becomes

$$Z \simeq \frac{1}{2}\left(\omega\tau_1 - \frac{2N}{\omega\tau_2} + \frac{A_I' E(N_D - N_A)}{\omega(1+\omega^2\tau_1^2)^{-1}}\right) . \quad (9)$$

In the high-frequency limit ($\omega\tau_1 \gg 1$), the mobility $\mu = e\tau_1/m_c$ is readily measured as $2Z = \omega\tau_1$.

In place of this simple model, a more precise calculation of $\hat{\sigma}$ can be made if $\omega\tau_1 \gg 1$. A first improvement to $\hat{v}$ is given by the many-valley model:

$$\frac{d\langle \vec{v}_j \rangle}{dt} = e\left(\frac{\vec{1}}{m}\right)\vec{E} - \left(\frac{\vec{1}}{\tau_1}\right)_j \langle \vec{v}_j \rangle , \quad (10)$$

where $1/\tau_1$ is replaced by a tensor

$$\left(\frac{\vec{1}}{\tau_1}\right)_j ,$$

which is diagonal in the principal axes of each valley (j). In general, the problem is not simple. In Appendix (A) the calculation of Z is derived in the simple cases of $\vec{E}$ parallel to the simple orientations $\langle 100\rangle$, $\langle 110\rangle$, or $\langle 111\rangle$. In the range of electric field under consideration and with the hypothesis of pure emission of acoustical phonons, $Z \simeq \frac{1}{2}\omega\tau_t$, where τ_t is the transverse relaxation time derived by Budd[21,22] from the many-valley transport theory at equilibrium.[23] A second improvement derives from an appropriate solution of the Boltzmann equation, from which $\hat{v}$ can be deduced.

A classical perturbation method in $1/\omega\tau_1$, with an isotropic effective mass m^* gives

$$Z = \tfrac{1}{2}\xi\omega\tau_1(kT_e) , \quad (11)$$

where the factor ξ depends on the shape of $f(\vec{p})$, the isotropic part of which is

$$f_0(\epsilon) \sim \exp[-(\epsilon/kT_e)^\delta] . \quad (12)$$

Table II gives the values of δ, ξ, and η such that $2Z = \eta\omega\tau_1(\langle\epsilon\rangle)$ in some simple cases. These results are applied in Sec. II A, which deals with the actual hot-electron problem [the calculation of $f(\vec{p})$ in a steady state]. Another interesting result comes from (9). The third term in the second member of (9) may be important with heavily doped samples (large values of $N_D - N_A$) and gives, through Z, some information on the impact-ionization rate. At the same time, some errors can occur because of this term even for a moderately doped sample if ω is not sufficiently high. If the impurity scattering is important, any sophisticated model, such as given by Appendix A, becomes useless, and in the case $\omega\tau_1 \gg 1$ the microwave mobility μ_m can be defined as $\mu_m = 2qZ/m_c\omega$, where m_c is the usual conductivity effective mass: $3m_c^{-1} = 2m_t^{-1} + m_l^{-1}$.

TABLE II. Correction to the microwave mobility μ_m with regard to the shape of $f(\vec{p})$. Acoustical scattering is supposed to be predominant with $\delta = 2.5$ or $\delta = 2$ (see text). The factor ξ is such that $2Z = \xi\omega\tau_1(kT_e)$ and η such that $2Z = \eta\omega\tau_1(\langle\epsilon\rangle)$.

Number of phonons (equilibrium)	δ	ξ	η
$\bar{N}_q \ll 1$	$\frac{5}{2}$	0.74	1.10
	1	0.33	0.5
$\bar{N}_q \gg 1$	2	0.95	1.20
	1	0.665	1.0

II. MOBILITY AND ELECTRONIC TEMPERATURE

The usual breakdown discussion is based upon observation of the $j(E)$ curves in dc and pulse measurements (Fig. 4). For a given sample, after a prebreakdown area in which the conduction process is very different (hopping transport), the current starts to rise at $E = E_c$. It increases by several orders of magnitude, until a saturation occurs and the slope of $j(E)$ decreases in the range $E > E_c$. We have measured the mobility from the lowest stable current at $T = 4\,^\circ$K($\sim 50\ \mu$A for the present samples) up to the saturation range, applying the perturbating cavity modes one after another. The invariability of μ_m is readily shown in Fig. 5, where ΔF and $F_0\Delta(1/Q)$ are seen to be linear functions of I. This invariability also occurs during the whole range of the current at $E = E_c$, with a discrepancy between the 4- and 35-GHz results that increases with the major impurity concentration (Figs. 6 and 7). In Fig. 6 μ_m is plotted versus j for sample (a) and in Fig. 7 all the results for samples (a)–(e) are summarized. Results for samples (d) and (e) are of no significance in terms of mobility. It is better to discuss them with the impact-ionization problem, since the main contribution to the factor Z for samples (d) and (e) comes from the third term of Eq. (9) (density modulation). Figure 8 gives the variations of $\mu_m(E)$ in the saturation for sample (a).

Theoretical comments upon these results are now given. We start from the most probable situation expected for hot electrons in pure samples at $T = 4\,^\circ$K, viz., the pure emission of acoustical phonons. The intervention of impurity scattering explains certain discrepancies between the results and the zero-point theory. The remaining discrepancies are discussed with the exact calculation of the acoustical-phonon limited mobility.

A. Interpretation with Zero-Point Approximation

The zero-point approximation,[21–24] or pure-emission limit, consists of setting $\bar{N}_q = (e^{qs/kT} - 1)^{-1} \ll 1$ in the calculation of the transition probabilities, i.e., in assuming a very large mean-free-carrier

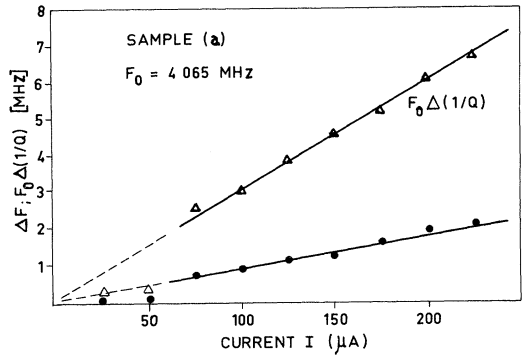

FIG. 5. $F_0\delta(1/Q)$ and δF_0 versus the total current I. In the lowest current range, an instability (see text) gives null variations of the mean shifts.

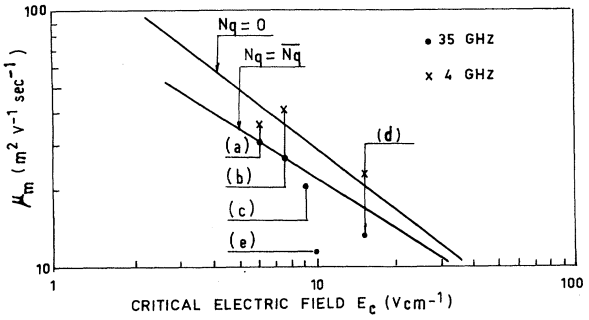

FIG. 7. In the whole range of j given in Fig. 6, the electric field is constant (E_c). The results for samples (a)–(d) are thus summed up for 4- and 35-GHz (crosses and dots) measurements and compared with some theories (see text).

power lost in phonon emission. It is a realistic assumption only if the time of measurement is very short compared to the corresponding phonon-heating time. We suppose as a first hypothesis that the pulse measurement has provided such a situation.

Stratton[25] has calculated the distribution function $f^S(\vec{p})$ for the relevant hot electrons, the isotropic part of $f^S(\vec{p})$ being

$$f_0^S \sim \exp[-(\epsilon/kT_e)^{5/2}] , \tag{13}$$

where $T_e \sim E^{0.8}$, and the mean energy calculated with (13) coincides with $1.5\ kT_e$. Budd[21,22] has calculated a hot-electron distribution function like (13) for each valley of many-valley semiconductors that takes into account elastic anisotropy. A tensor $(\overleftrightarrow{1/\tau})$ can be calculated and the solution (13) in each valley is given by

$$(kT_e)^{5/2} \sim \frac{H^2\Sigma_4^4}{\Sigma_t^2\Sigma^{*2}} E^2\left(\sin^2\alpha + \frac{m_t\tau_l}{m_l\tau_t}\cos^2\alpha\right). \tag{14}$$

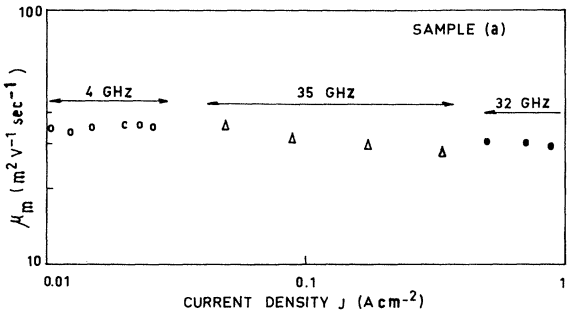

FIG. 6. Microwave mobility μ_m versus the mean current density j; the empty circles, triangles, and filled circles are, respectively, the data at 4, 35 (015), and 32 GHz (014).

Σ^* and Σ_t are new deformation potentials introduced in Ref. 21, $(\overleftrightarrow{1/\tau}) = \mathrm{diag}\,(\tau_t^{-1}, \tau_t^{-1}, \tau_l^{-1})$ the inverse relaxation tensor in the principal axes of the valley, α the angle (E, z axis), s_l the sound velocity of longitudinal phonons, and H a numerical factor such that $\tau = H\epsilon^{-1}$ in the simple spherical model built with the constants m^* and Σ_d. Using the usual n-type Ge constants, we have

$$\tau_t = 2.2\times10^{-11}\epsilon^{-1}\ , \quad \tau_l/\tau_t = 1.6\ . \tag{15}$$

If $\vec{E}$ is along $\langle 100\rangle$, the four electronic temperatures are given by

$$kT_e = 0.94E^{0.8}\ . \tag{16}$$

In both (15) and (16) the energies are calculated in units of $\epsilon_i = 2\times10^{-21}$ J (impurity ionization energy of As centers) and E in units of 10 V cm^{-1}.

Now we return to the consistency of the zero-point approximation. $\langle p\rangle\, s \gg kT$ implies

$$T_e/T \gg kT/3m^*s^2\ . \tag{17}$$

For $T = 4\,^\circ$K, (17) is equivalent to $T_e \gg 10\,^\circ$K, i.e., $E \gg 1$ V cm^{-1}, if E is parallel to $\langle 100\rangle$, and expressions (13)–(16) may be quite accurate for $E \geq 6$

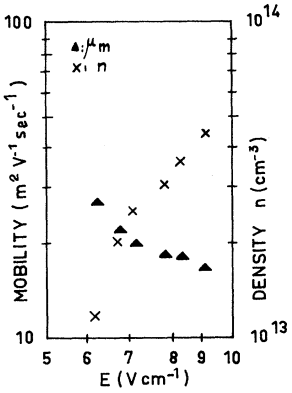

FIG. 8. $\mu_m(E)$ in the saturation range for sample (a) (TE014 mode). The corresponding values of $n(E)$ are also given as $j \simeq ne\mu_m E$.

V cm^{-1} and $T \leq 4.2$ °K. Even if consistent, the zero-point approximation has to be checked with respect to other inelastic scatterings, such as optical phonons, ionization collisions, and interelectronic processes. These details have been reported in Appendix B, the important features of which are (i) that optical phonons do not intervene if $E < 30$ V cm^{-1} ($T = 4$ °K), (ii) that impact-ionization collisions do not modify the distribution as long as $N_D - N_A < 10^{15}$ cm^{-3} and $E \sim E_c$, as pointed out earlier by Zylbersztejn, who used other hypotheses,[2] and (iii) that the interelectronic process is weak compared to acoustical scattering if $n < 10^{14}$ cm^{-3}.

The theoretical value of μ_m occurring in Eqs. (15) and (16) is given by the solid line in Fig. 7. The difference of 30% between the mm wavelength measurements and the above theory is significant for samples (a)–(c) and the divergence is higher for sample (a) in saturation (the absolute value of the slope $\log\mu_m/\log E$ is higher than 0.8). Both the impurity scattering and the phonon departure from equilibirum can be invoked.

B. Role of Impurity Scattering

Two kinds of impurities can limit the mobility: neutral impurities, in number $(N_D - N_A - n)$, and ionized impurities, in number $(2N_A + n)$. For neutral impurities the Erginsoy formula[26] gives

$$\mu_n = 250(N_D - N_A - n)^{-1}, \tag{18}$$

where the concentrations are measured in units of 10^{14} cm^{-3} and the mobility in m^{2}V^{-1}sec^{-1}. In Table III the partial mobility μ_n is listed for $n \ll (N_D - N_A)$. It also includes the partial mobility μ_i (ionized impurities) deduced from the (generalized) Brooks–Herring formula.[27]

When impurity scattering occurs, Eq. (16) is no longer valid, and a new calculation of the mean energy must be made:

TABLE III. The microwave mobility μ_m measured in the mm wavelength range is close to the drift mobility. Theoretical mobilities are then compared with μ_m. The mean energy $\langle\epsilon\rangle$ deduced from Eqs. (20), (B3), and (B4) is normalized to ϵ_i, taking account of the difference between As and Sb centers.

		Theoretical mobilities (m^2 V^{-1} sec^{-1})				
Sample	E_c (V cm^{-1})	μ_a	μ_i	μ_m	μ_m (35 GHz)	$\frac{\langle\epsilon\rangle}{\epsilon_i}$
(a)	6.1	43	>500	330	30	0.65
(b)	7.5	35	300	145	25.5	0.50
(c)	9	30	300	110	21	0.6
(d)	15	20	200	65	13	0.7
(e)	10	28	200	40	11.5	0.7
(f)	55	7	···	3.7	···	0.85
(g)	65	6	···	2.2	6	0.7

$$e\mu E^2 = \langle d\epsilon/dt\rangle_a + \langle d\epsilon/dt\rangle_{i0}, \tag{19}$$

where $\langle d\epsilon/dt\rangle_a$ and $\langle d\epsilon/dt\rangle_{i0}$ are the mean power lost by one electron with acoustical-phonon and ionization collisions, and μ is given by Eq. (15). In Appendix B the values of $\langle d\epsilon/dt\rangle_a$ and $\langle d\epsilon/dt\rangle_{i0}$ are estimated, and from Eq. (19) with the measured value of μ_m, the mean energy $\langle\epsilon\rangle$ is deduced. The result $\langle\epsilon\rangle \sim 0.7\epsilon_i$ at $E = E_c$ is verified with both arsenic and antimony centers.

The large values of μ_i obtained for samples (a)–(c) yield the intervention of another phenomenon during the saturation range for sample (a) (Fig. 8), as we shall see now.

C. Precision on Phonon Scattering

Conwell[12] and Zylbersztejn and Conwell[13] have shown the important role played by the phonon effects (size dependence of the mobility) in the saturation. In Refs. 12 and 13 the following hypotheses were made: The distribution function is Maxwellian, the avalanche saturates ($n \rightarrow N_D - N_A$) and the mean free path for the phonons are only limited by the sample boundaries, i.e., the lifetime of a given phonon τ_q is $\sim d/s$, where d is the smallest width of the sample. In the present case, d is rather low and the expected phonon heating effect is weak. Thus a precise calculation of the perturbation to the zero-point theory is made by using the exact solution of the coupled system, the distribution function being calculated exactly. The mobility has been measured at 0.5 μsec after the beginning of the avalanche process. This time is long enough to permit a correct steady-state analysis for $\tau_q \sim 10^{-7}$ sec ($d = 0.05$ cm and $s \sim 5\times 10^5$ cm/sec). Even with $N \sim \bar{N}_q$, the problem is not simple, and a numerical computation of the mobility is needed. The general problem consists of solving two coupled Boltzmann equations. To avoid excessive complexity, we assume a simple isotropic band model with $m^* = 0.22m_0$ and E_1, a deformation potential that is adjusted by experiment. This point of view is different from the first paragraph of Sec. II A where the exact theoretical value of μ_m was compared with the experimental value, which is only possible with either $N_q = 0$ or $N_q \gg 1$. The coupled system is

$$e\vec{E}\cdot\vec{\nabla}_p F = \frac{E_1^2 m^*}{4\pi\rho s\hbar^4 p}\left(\int_0^{2p}[(N_q+1)f_0(p+q) + N_q f_0(p-q) - (2N_q+1)f_0(p)]\,q^2\,dq\right), \tag{20a}$$

$$\frac{N_q - \bar{N}_q}{\tau_q} = \frac{E_1^2 m^*}{2\pi\rho s\hbar^4}\left(\int_{q/2}^{\infty}[(N_q+1)f_0(p) - N_q f_0(p-q)]\,p\,dp\right). \tag{20b}$$

$f_0(\epsilon)$ is the isotropic part of $f(\vec{p})$ and we are interested only in the isotropic part of N_q. The diffusion approximation yields

$$f(\vec{p}) = f_0(\epsilon)[1 + w(\epsilon)\cos\theta] , \tag{21}$$

with $w \ll 1$. If only acoustical scattering is present,

$$f_0(\epsilon) \sim \exp\left(- \int_0^{\epsilon} \frac{w(\epsilon')d\epsilon'}{eE\lambda(\epsilon')} \right) , \tag{22a}$$

$$\frac{1}{\lambda} = \frac{1}{v} \frac{E_1^2 m^*}{4\pi\rho s\hbar^4 p} \int_0^{2p} (2N_q + 1) q^2 dq . \tag{22b}$$

Equation (22a) is the solution given by (21) and (20a) and corresponds to a useful change of variable introduced by Keldysh.[28] For $N_q = \bar{N}_q$ the system (20) is decoupled and Eqs. (22a) and (20) give $w(\bar{N}_q)$ and f_0. The mobility is then $\mu = \langle \vec{v} \rangle / \vec{E}$. The problem of n-type Ge can be rewritten with normalized parameters:

$$N(z, x) = \bar{N} + P \frac{\int_z^{\infty} \exp[-\varphi(x')]\, dx'}{\int_0^{\infty} \exp[-\varphi(x')]\sqrt{x'}\, dx'} , \tag{23a}$$

$$\varphi(x) = \frac{\alpha}{c} \int_0^x w(x')\sqrt{x'} \int_0^1 (2N + 1) z^2 dz , \tag{23b}$$

where $x = \epsilon/\epsilon_i$ (normalized energy) and P is a parameter proportional to the electronic density and the coupling strength:

$$P = \frac{\pi}{2} \frac{\tau_q n E_1^2 (2m^*)^{1/2}}{\sqrt{\epsilon_i}\, \hbar \rho s} . \tag{24}$$

For acoustical phonons $w(\epsilon)$ is independent of N_q: $w(x) = 0.75x/c$, where the parameter c is a normalized electric field, $c = E/E_0$, and α is a corresponding numerical factor, and both are functions of E_1. The choice of E_1 has been made in the following way. In (23) we take $N = \bar{N}$ ($P = 0$, $T = 4.2\,^{\circ}\mathrm{K}$) and the resulting mobility is compared with the experimental value at $E = E_c$ for sample (a), with several values of E_1. The best fit is obtained with $E_1 = 13.5$ eV. Thus it gives $\alpha = 13$, $E_0 = 8.5\ \mathrm{V\,cm^{-1}}$, and $P = 4dn$, where d is measured in cm and n in units of $10^{14}\ \mathrm{cm^{-3}}$. The complete calculation with arbitrary values of P is then developed from the solution $N = 0$, by the iterative process $P = 0.1$, and $N = 0$ in (23b) $\rightarrow \varphi_0 \rightarrow N_1(\varphi_0)$ by (23a), etc.; $P = 0.2$, and N is given by the preceding result ($P = 0.1$), etc.

The iteration converges within the electric field range $5 < E < 50\ \mathrm{V cm^{-1}}$ and $x < 10$. In Fig. 9 the theoretical curves $\mu(E)$ are drawn on a linear scale for some values of P. If one compares these curves with the experimental results, the situation is qualitatively quite satisfactory (see the lower curves in Fig. 9), since the experimentally measured values of P increase linearly with n(n is deduced from both j and μ). However the value of $P = 4dn$ would be only 0.2 times the measured value for $d = 0.04$. This discrepancy is perhaps explained by the following considerations:

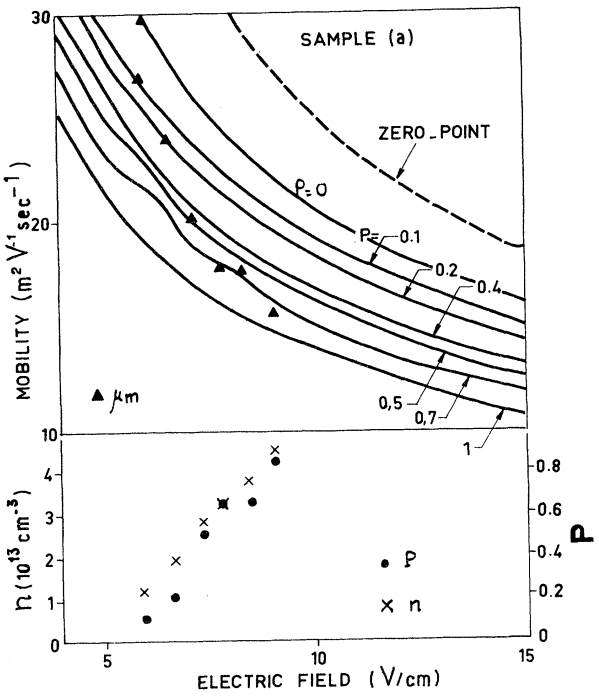

FIG. 9. Theoretical interpretation of $\mu_m(E)$ in the saturation range. $\mu_m(E)$ has been calculated by an iterative process (see text) and the theoretical results (solid curves) are drawn for several values of the parameter P, which is proportional to n. Experimental values of $P(E)$ are deduced from the upper curves and experimental values of μ_m, both results and theory being fitted at $P = 0$ by the choice of E_1 (see text). In the lower part of the figure, $n(E)$ and $P(E)$ are compared.

(i) Partially specular reflection at the sample surface, which implies $\tau_q > d/s$.

(ii) The phonons propagating along $\vec{E}$ are not damped by the boundaries; for these phonons, stimulated emission can occur as the drift velocity exceeds the sound velocity.[29]

(iii) The heat injected at the cathode (where n is very high) propagates along the direction $\langle 100 \rangle$ essentially with transverse phonons ($\Sigma_{\mu} = 19$ eV). These extra phonons may add to the intrinsic heating process and to the stimulated emission process. This point is verified by other experiments with a scanning of the microwave probe along the sample.[16]

The best approximation is thus the zero-point limit (within 30%) for hot electrons during breakdown of n-Ge. The results of experiments reported in Ref. 1 suggested higher electronic temperatures than those of our results, but with the exactly opposed hypothesis ($N_q \gg 1$). Moreover, as

the lattice temperature was rather high, the electrons were not even as hot as in the present case and impurity scattering was, of course, rather important. However, for moderate electric fields, both results are of the same order. Further consideration of the coupled hot-electron–hot-phonon problem requires a time-and-space analysis of the whole system that takes into account the contact effects. A simple analysis of the impact-ionization problem (Sec. III) can thus only be made by using a very short time of measurement (inferior to the phonon heating characteristic time) ($\sim \tau_0$).

A significant anisotropy of the mobility can be predicted (see Appendix A). However the main effect is a variation of E_c, as previously shown in Ref. 1, and the average mobility is not very different since the stronger field dependence of μ is partly compensated by the lower effective mass of the hotter valleys.

III. IMPACT-IONIZATION PROBLEM

A. Transient Technique to Measure A_I

The very simple electrical circuit in which the sample is inserted consists of two coaxial cables with a pulse generator on one side and a load R on the other side (see Fig. 10). The generator develops a step of voltage V_1 that remains approximately constant after $t=0$. The voltage $V_2(t)$ across R is proportional to the current $I(t)$, owing to some impact-ionization process, and, if one neglects contact phenomena, the electric field $E(t)$ is $(V_1 - V_2)/l$, where l is the distance between the two Ohmic contacts. At $t=0$, $V_2=0$ and dV_2/dt are positive if $V_1/l > E_c$. The subsequent evolution of V_2 is described by Price's model,[20] i.e., Eq. (7), in which we disregard the thermal generation rate, which is negligible for $T < 10\,^\circ$K. One has to write the external circuit condition:

$$V_1 = \text{const} = E(t)l + eRSv(E)w(t) \,, \tag{25}$$

where l is the sample length, S the cross section, and v the drift velocity for the applied electric field. The log derivative of (25) yields

$$\varphi = \frac{1}{V_2}\frac{dV_2}{dt} = \frac{l}{l + mRS\sigma}\frac{1}{n}\frac{dn}{dt} \,, \tag{26}$$

where m is the exponent entering in $v(E) \sim E^m$ ($m = 0.2$ for the zero point of acoustical phonons) and σ is the dc conductivity for the chosen current and depends on the resistance R and V_1. For a fairly pure sample the condition $l \gg mRS\sigma$ can be easily realized, so that $V_2(t)$ and dV_2/dt describe the density $n(t)$ and dn/dt [given by Eq. (7)], provided that the relevant response time of the present problem remains much larger than the energy relaxation time τ_2 (~ 0.5 nsec for n-type germanium). Thus the signals $V_2(t)$ and dV_2/dt can lead to the kinetic parameters entering Eq. (7). The maximum value of dV_2/dt is particularly interesting. If one writes $d^2V_2/dt^2 = 0$ by means of (25), (7), and (26), with $l \gg mRS\sigma$, simple relations between φ and the kinetic parameters can be derived for the precise time when dV_2/dt is maximum.

(i) If $n \ll N_A$, the maximum value of dV_2/dt is obtained exactly for $n_M = \frac{1}{2}n_\infty$, where n_∞ is the steady-state value reached by n when $t \to \infty$, and

$$\varphi_M = \tfrac{1}{2}[A_I(E_M)(N_D - N_A) - B_T(E_M)N_A] \,. \tag{27}$$

(ii) If $n \gg N_A$, the parameters at the maximum of dV_2/dt are given by

$$n_M = \frac{n_\infty}{\sqrt{3}} \,, \quad \varphi_M = \tfrac{2}{3}[A_I(E_M)(N_D - N_A) - B_T(E_M)N_A] \,. \tag{28}$$

The electric field E_M is readily deduced from V_1 and the value of V_2 for the maximum of dV_2/dt.

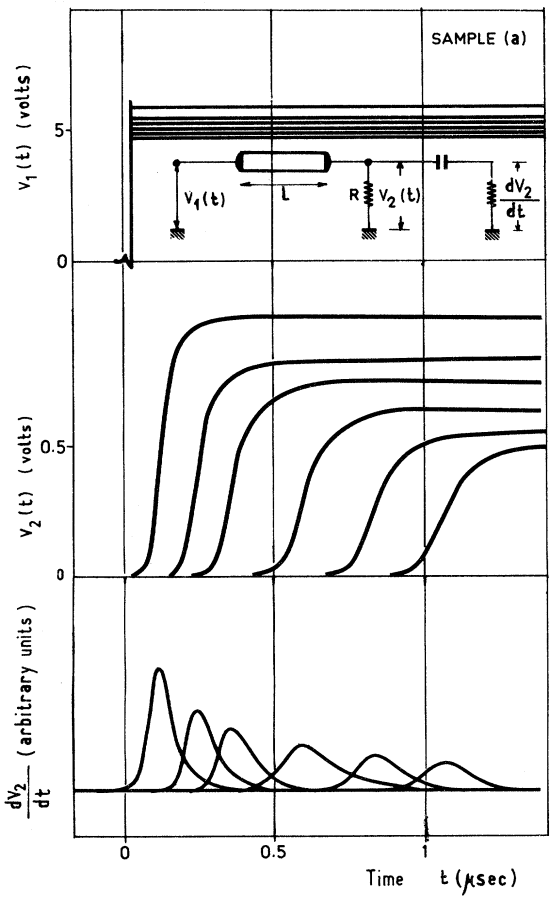

FIG. 10. Electrical scheme of the present experiment is shown on the upper figure with the total applied voltages V_1 versus time (steps). A current proportional to V_2 (middle figure) is obtained after a certain delay time and with a certain rise time, which is the main object of our study. The lower curves present dV_2/dt and have a maximum, which is an interesting parameter, with respect to the electric field $E(t) \sim (V_1 - V_2)/l$.

Since the recombination parameter B_T decreases with E and the impact-ionization rate A_I steeply increases with E immediately above E_c, we arbitrarily drop the recombination contribution in the second members of Eqs. (27) and (28).

The ideal situation described above deals with a homogeneous, instability free, avalanche breakdown phenomenon. It does not take into account the parasitic phenomena which may accompany the lowest-temperature impact ionization. Koenig[30] has already explained the delay time between the step V_1 and the current response V_2 in terms of a contact effect. The "delayed breakdown" can be easily suppressed by application of a weak dc current superimposed to the pulses. Another phenomenon that can occur is heat injection at the cathode. This problem itself is beyond the scope of the present paper, and up to now we suppose that the heat injection produces no important effect if the heat propagation time along the sample is long compared to the analyzed avalanche rise time, i.e.,

$$\tfrac{1}{2}A_I(N_D - N_A) \gg s/l \,. \tag{29}$$

For a typical sample this condition is easily realized if $l > 1$ mm and $N_D - N_A > 5\times 10^{13}$ cm^{-3}. Experimental values of $A_I(E)$ deduced from (27) and (28) with the purer As- and Sb-doped samples [(a) and (c)] are plotted in Figs. 11 and 12. The extrapolated value of $A_I(E)$ at $E = E_c$ meets the previously deduced value for the Sb-doped sample.[1] The present method can be applied without difficulty to other transient phenomena of the same (apparent) behavior.

B. Theoretical Calculation of $A_I(E)$

The impact-ionization cross section of impurity atoms is a complex problem for many-valley semiconductors since many parameters enter the different matrix elements. Moreover, the measured parameter $A_I(E)$ itself is an average over the distribution function $f(\vec{p})$, $A_I = \langle \sigma_i(\epsilon) v \rangle$, and any good idea about $\sigma_i(\epsilon)$, at least within an order of magnitude, strongly depends on the choice of $f(\vec{p})$.

We have shown in Sec. II that the zero-point hypothesis is valid within 30% for electric fields $E \gg 1$ V cm^{-1}, but in no way does it imply that $f(\vec{p})$ is close to expression (13) in the whole range of ϵ: the ratio $f_1/f_0 \sim \epsilon$ and the Legendre's expansion become invalid for large values of ϵ. The exact calculation of distribution functions in semiconductors is of growing interest, and we report the method used in the present problem, which follows the numerical iterative procedure due to Budd.[31,32] An equivalent expression of the Boltzmann Eq. (21) is

$$f(\vec{p}) = \int_{-\infty}^{0} \left[\exp\left(\int_0^t \frac{dt'}{\tau(t')} \right) \right] \underline{O}\, \{ f(\vec{p}^{\,*}) \}\, dt \,, \tag{30}$$

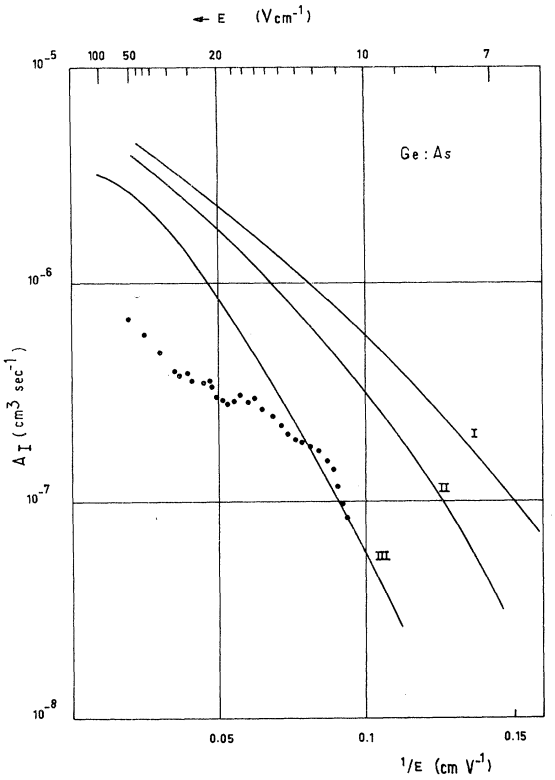

FIG. 11. Semilog plot of the impact-ionization rate A_I versus $1/E$. The experimental points of measurements for sample (c) (As doped) are compared to three theoretical laws: (I) in which the cross section is constant and the zero-point distribution function is used; (II) with the same constant cross section, but with introduction of an equilibrium distribution of phonons $\bar{N}_q$; (III) with the distribution function of (II), but now with an hydrogenlike cross section.

where $1/\tau$ and $\underline{O}$ are the relaxation time and operator given by (22) and $\vec{p}^{\,*} = \vec{p} + e\vec{E}t$ is the solution of the collision-free problem. An analysis of (30) has been made by Chuenkov,[6] who has shown that $f(\vec{p})$ is needlelike when $\epsilon \gg \epsilon_i$ for $E \sim 10$ Vcm^{-1} in n-Ge. However, the calculation made in Ref. 6 neglects the important angle dependence of the operator $\underline{O}$ when $N_q = 0$. In fact, the transition probabilities for electron-phonon collisions are

$$W_e \sim (1 + N_q) q \quad \text{(emission)} \,,$$

$$W_a \sim N_q q \quad \text{(absorption)} \,.$$

At high temperatures, W_e and W_a become independent of q as $N_q \sim kT/qs$. At the lowest temperatures they are, however, proportional to q and the large-angle ($\theta > \frac{1}{2}\pi$) scattering is predominant. The numerical solution of (30) is easy for $N_q \ll 1$ since the exponential term can be calculated explicitly: $\tau^{-1}(\epsilon^*) \sim \epsilon^*(t)$. The numerical solution for (30) is an iterative process from the Stratton's distribution

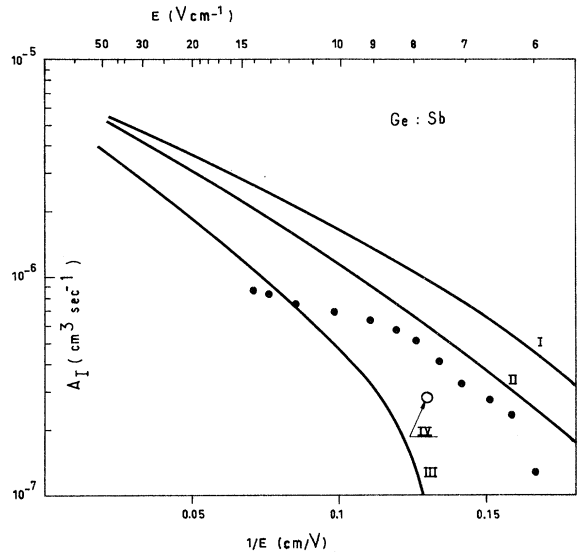

FIG. 12. Same results and theories as in Fig. 11 for Sb-doped samples. Results of sample (a) are plotted. It also includes a theoretical point (IV) that is deduced from the exact calculation of the distribution function.

function $f_0^s(\epsilon)$. The results are given in Figs. 13 and 14. In Fig. 13 the first three projections of $f(\vec{p})$ on Legendre polynomials are drawn and compared with f_0^s. For the large energy limit ($\epsilon \gg \epsilon_i$), the values

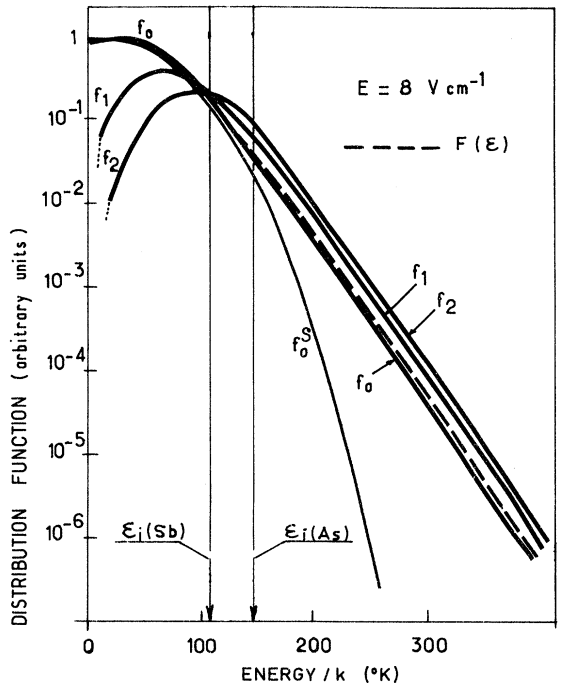

FIG. 13. Exact calculation of $f(\vec{p})$ expanded in Legendre polynomials. The three first projections are represented in this figure and compared to f_0^s and $F(\epsilon)$.

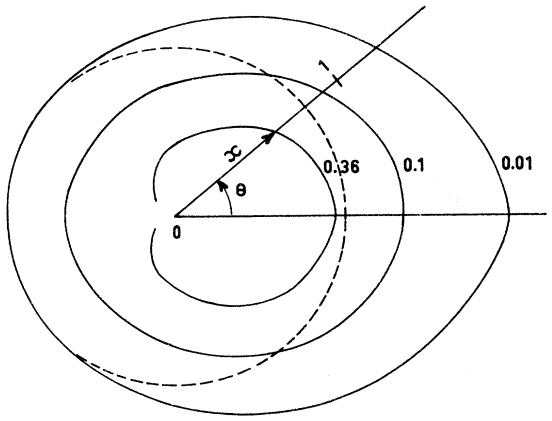

FIG. 14. Distribution function of Fig. 13, on a polar diagram, θ being the angle $(\vec{p}, \vec{E})$ and the radius vector is $x = \epsilon/\epsilon_i$. The lines of equiprobability are plotted ($f = 0.36$, 0.1, and 0.01). It is compared to the zero-point theory, ($f_0^s = 0.36$, dashed line).

of f_0, f_1, and f_2 are nearly all the same but very different from f_0^s, in good agreement with the needlelike assertion.[6] The physical significance of that result already has been pointed out by Shockley.[33] The probability $F(\epsilon)$ that an electron obtains an energy $\epsilon \gg \langle \epsilon \rangle$ is close to the probability that an electron would be accelerated by the field E on a length z such that $\epsilon = eEz$, i.e., $F \sim e^{-z/\Lambda}$, where Λ is the mean free path. Now, if the free path is energy dependent, e.g., $\lambda(\epsilon)$, it is easy to show that

$$F(\epsilon) \sim \exp\left(-\int_0^{\epsilon} \frac{d\epsilon'}{eE\lambda(\epsilon')} \right), \tag{31}$$

which is just the solution derived by Chuenkov[6] through the analysis of (30). Although it is valid at far higher energies ($\epsilon \gg \epsilon_i$), solution (31) cannot be applied for the present problem. The difficulty is merely shown by the direct representation of $f(\vec{p})$ on a polar diagram (Fig. 14). It is clear that over the relevant energy range ($\epsilon_i < \epsilon < 2\epsilon_i$), a needlelike distribution function is not displayed at $E \sim 10$ V cm^{-1}, and this is probably true at higher electric fields.

The generation rate $A_I(E)$ is directly related to $\sigma_i(\epsilon)$ by $A_I = \langle \sigma_i(\epsilon) v \rangle$. Since $f(\vec{p})$ decreases steeply for $\epsilon > \langle \epsilon \rangle$ (see Fig. 13), the problem consists of knowing the actual dependence of $\sigma_i(\epsilon)$ immediately above ϵ_i. With that point of view, the simplest choice for σ_i is[2]

$$\sigma_i(\epsilon) = 0, \qquad \epsilon < \epsilon_i$$
$$= \sigma_0 \text{ const}, \quad \epsilon > \epsilon_i . \tag{32}$$

For high energies, $\sigma_i(\epsilon)$ decreases as $1/\epsilon$, as deduced from the usual Bethe formula with impact ionization of hydrogen atoms. Near ϵ_i, the ex-

perimental law for atomic hydrogen gives a linear increase if $\epsilon \sim 2\epsilon_i$, a maximum value of $\sim 0.8\pi a_0^2$ (a_0 is the Bohr radius), and if $\epsilon \gg \epsilon_i$, $\sigma_i \sim 1/\epsilon$. The theoretical proof of the validity of such a linear increase of $\sigma_i(\epsilon)$ has been given by Keldysh,[34] the discrepancy being high for large values of K_R [in which case the theory of Keldysh gives $\sigma_i(\epsilon) \sim (\epsilon - \epsilon_i)^2$]. A second simple choice of $\sigma_i(\epsilon)$ is thus

$$\begin{aligned} \sigma_i &= 0, && \epsilon < \epsilon_i \\ &= \sigma_0(\epsilon - \epsilon_i)/\epsilon_i, && \epsilon_i < \epsilon < 2\epsilon_i \\ &= 2\sigma_0\epsilon_i/\epsilon, && \epsilon > 2\epsilon_i . \end{aligned} \tag{33}$$

The maximum value σ_0 may be close to the Bohr section. For a many-valley semiconductor, we choose $\sigma_0 = \pi(a^2 b)^{2/3}$, where a and b are the half-axes of the envelope wave function.

The values of ϵ_i, a, and b are given by Table IV; the triplet state, occupied at $T = 4\,^\circ$K, has been chosen as the ground state for the Sb centers.

Three theoretical curves have been drawn on Figs. 11 and 12.

(I) $f(\vec{p})$ is the zero-point limit distribution function in the many-valley case with E along $\langle 100 \rangle$ and $\sigma_i(\epsilon)$ determined by (32).

(II) $f(\vec{p})$ is deduced from a rigorous calculation of the acoustical scattering [Eqs. (21) and (22)], with $E_1 = 13.5$ eV and $m^* = 0.22\, m_0$ to fit the experimental values of μ, always with $\sigma_i(\epsilon)$ given by (32).

(III) $f(\vec{p})$ is the same as in (II) but now $\sigma_i(\epsilon)$ obeys the law (33).

For the (As) impurity (Fig. 11) the determination (III) is very close to the experimental results for moderate electric fields. It is probably fortuitous but the agreement is good with regard to the order of magnitude and, mainly, to the slope of $A_I(E)$. For higher values of E, the problem has to be entirely reconsidered, since the impact-ionization process itself may modify the distribution function (see Appendix C). The obvious result is a decrease of the absolute value of $\ln(A_I)E$, corresponding to a slower variation of T_e with E than would be predicted from acoustical scattering alone.

For Sb centers, the quantitative agreement is not so good, but the experimental slope of $A_I(E)$ also follows (III). The question of the high-energy tail arises primarily because the electric field is somewhat less than for As centers. The computation of $A_I(E = 8\ \mathrm{V\,cm^{-1}})$, with the exact tail shown on Figs. 13 and 14, and of (33) for σ_i, gives a determination (IV) that agrees with the experimental results slightly better than (III). However the very large difference of A_I for As- and Sb-doped samples predicted by all the theories is reflected in the experimental results, which show that impact ionization concerns the direct transition from the ground state into the conduction band with no phonon-assisted cascade process, as in the recombination.[7] The maximum of the impact-ionization cross section is of the order of σ_0, but the variation is perhaps steeper than $(\epsilon - \epsilon_i)$ [perhaps $(\epsilon - \epsilon_i)^{1/2}$]. The reason why a law such as $\sigma_i \sim (\epsilon - \epsilon_i)^2$ would be incorrect is that the impulse approximation used in Ref. 34 is a poor approximation for the impact-ionization problem.

TABLE IV. Properties of the ground state for As and Sb centers and order magnitude of $A_I^0 \sim \pi a_0^2 v(\epsilon_i)$.

Sample	$N_D - N_A$ ($\mathrm{cm^{-3}}$)	ϵ_i (meV)	a (A^0)	b (A^0)	$\pi a_0^2 v(\epsilon_i)$ (10^{-6} $\mathrm{cm^3\,sec^{-1}}$)
(a) (Sb)	6×10^{13}	9.0 (T)	72.0	16.2	3.7
(c) (As)	2×10^{14}	12.7	60.5	13.6	4.4

We can now discuss the impact-ionization contribution to the factor Z, which increases with increasing $(N_D - N_A)$ and decreasing ω. The percentage of the third term of Eq. (9) over its first term, i.e., the density modulation rate over the velocity modulation rate, is listed in Table V. For samples (f) and (g) that percentage is assumed to be $\sim 100\%$ at $F_0 = 4$ GHz. Hence one can calculate $A_I' E$ for samples (f) and (g) from Z, neglecting the mobility contribution. It gives $A_I' E \sim 10^6\ \mathrm{cm^3 sec^{-1}}$, and can be compared with the experimental value of $A_I(E)$ for a moderately doped sample ($A_I' E \sim 10^6\ \mathrm{cm^3 sec^{-1}}$ for $E \sim 10\ \mathrm{V\,cm^{-1}}$).

C. Hot-Electron Recombination Time

In Eq. (7), the steady state yields $dn/dt = 0$, i.e., the balance between the impact-ionization rate and the thermal and Auger reciprocal processes (thermal ionization can be neglected). The Auger recombination parameter for hot electrons can be deduced from the main experimental results of the present work, i.e., from $n(E)$ and $A_I(E)$. Lax's theory,[7] involving the giant-traps effect, gives a sharp dependence of B_I on E in the hot-electron regime. The recombination probability for a single electron of given energy $\epsilon \gg kT$ has been calculated in Ref. 7:

$$\sigma_R(\epsilon) \sim \frac{1}{\epsilon T^4 (\epsilon + 6kT)^3} \exp \frac{9kT}{\epsilon + 3kT} . \tag{34}$$

We now assume that the same dependence is valid for the Auger process. The parameter B_I is thus $B_I \sim \langle \sigma_R(\epsilon) v \rangle$. With the hot-electron distribution function $f_0^S(\epsilon)$, the high-energy dependence of B_I cannot be calculated explicitly, except in the very-hot-electron range $\epsilon \gg 10kT$, in which case $\sigma_R \sim \epsilon^{-4}$ and thus $B_I \sim T_e^{-3.5} \sim E^{-2.8}$. In the present case, $\langle \epsilon \rangle \sim 10kT$, and the expected law $B_I(E)$ is between $\sim E^{-2.8}$ and $\sim E^{-2.3}$ (the latter is shown by Koenig *et al.*[1] in prebreakdown measurements of B_T).

The balance equation gives, for $n > N_A$,

$$B_I n^2 \simeq (N_D - N_A - n) A_I ,$$

and the knowledge of $A_I(E)$ and $n(E)$ [sample (a)] leads to $B_I(E)$, which is plotted in Fig. 15. The experimental slope gives $B_I \sim E^{-2.5}$. A quantitative comparison can be drawn: The extrapolation of $B_I(T_e)$ down to $T_e = 6\,^\circ$K agrees with the previous result of Koenig *et al.*[1] for equilibrium electrons ($B_I \sim 0.7 \times 10^{-17}$ cm^6 sec^{-1} at $T_e = T = 6\,^\circ$K). The two lines of slope -2.5 in Fig. 15 start from the points $T_e = T = 6\,^\circ$K and $T_e = T = 4\,^\circ$K with the results of Ref. 1.

The agreement is thus quite satisfactory. The hot-electron and cold-electron recombination parameters thus differ by two orders of magnitude, which agrees well with the giant-trap law.

CONCLUSION

New experimental results concerning the impact-ionization problem have been presented for impurity breakdown in n-Ge. The acoustical scattering theory has been extensively discussed and an original calculation of the coupled Boltzmann equations has been given. A time-dependent study of the coupled electron-phonon system will be given in another paper. The impact-ionization cross section is in good agreement with the classical H-atom results and the slope of $A_I(E)$ confirms the validity of the distribution function used in the mobility discussion. The Auger process becomes important as $n > 10^{13}$ cm^{-3} and the present result agrees with former cold-electron data of Koenig *et al.*[1] and with the giant-traps theory.

It would be interesting to study what happens in a transverse magnetic field, since the giant orbits thus involved may be modified. Details on this point will be given in another paper.[16] Impurity scattering and many-valley effects seem to be of secondary importance in the present paper. The first acts only on the mobility, primarily by the number of neutral centers, and increases the avalanche generation rate, and the second has been avoided by the chosen ⟨100⟩ orientation for the applied electric field. It is expected in any case that the many-valley effect is of secondary importance during breakdown, since impurity scattering redistributes the electronic temperatures in a time shorter than the smallest time involved in the present experiments.

TABLE V. Importance of the density modulation [see Eq. (9)]. The different terms of the third and fourth columns have been estimated by assuming $Z = A_I' E_c (N_D - N_A)/2\omega$ for the heavily doped sample (g) at 4 GHz.

Sample	$\langle Z \rangle$ (4 GHz)	$\langle Z \rangle$ (35.5 GHz)	$\frac{A_I' E_c (N_D - N_A)}{2\omega \langle Z \rangle}$ (4 GHz)	$\frac{A_I' E_c (N_D - N_A)}{2\omega \langle Z \rangle}$ (35.5 GHz)
(a)	0.30	2.9	$\sim 0.5 \times 10^{-2}$	$\sim 10^{-3}$
(b)	0.35	2.5	$\sim 10^{-2}$	$\sim 2 \times 10^{-3}$
(c)	...	2.0	...	$\sim 2 \times 10^{-3}$
(d)	0.20	1.25	3×10^{-2}	5×10^{-3}
(e)	...	1.1	...	8×10^{-3}
(f)	0.15	...	0.75	...
(g)	0.45	~ 0.6	1	~ 0.1

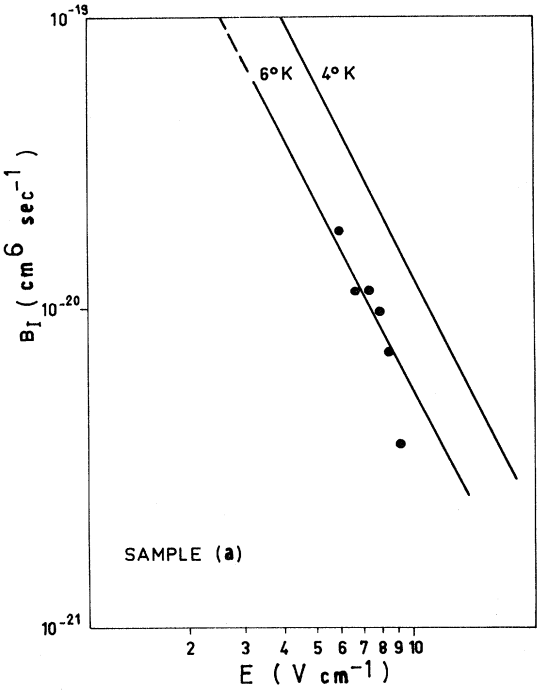

FIG. 15. Auger recombination parameter B_I versus E in the saturation range. The solid lines are extrapolations of the results given in Ref. 1 for $T_e = T = 6$ and 4 °K with a slope -2.5 (log-log scale).

ACKNOWLEDGMENTS

We are indebted to G. Dupas for his technical assistance during experiments. We wish to thank Dr. H. F. Budd whose encouragements and theoretical guidance have been greatly appreciated. We also thank Dr. J. Bok, Dr. J. Tavernier, Dr. A. Zylbersztejn, Dr. M. Camus, Dr. H. A. Combet, Dr. C. Vassallo, Dr. R. K. Kar, and Dr. J. P. Maneval for fruitful discussions. We thank J. Yhuel for the computation of $f(\vec{p})$, J. Frère for the sample cutting, and J. C. Brault for the delicate cavities.

APPENDIX A

The simple model based upon Eqs. (3) and (4) can be generalized in the many-valley case. Generalization of Eq. (3) yields the tensorial form given by (10). In (10) the energy relaxation effects have been neglected (which is valid in the limit $\omega\tau_1 \gg 1$). We can define a microwave mobility matrix relative

to the valley (j):

$$\vec{\hat{\mu}}_j = \mathrm{diag}(\hat{\mu}_{tj}, \hat{\mu}_{tj}, \hat{\mu}_{lj}) , \tag{A1}$$

with

$$\hat{\mu}_{tj} = \mu_{t0j}(1 + i\omega\tau_{tj})^{-1}, \qquad \mu_{t0j} = e\tau_{tj}/m_t , \text{ etc.}$$

The transverse and longitudinal relaxation times τ_{tj} and τ_{lj} have been introduced by Budd,[21,22] and are functions of the electronic temperature T_j of each valley (j) which itself depends upon the orientation and intensity of the steady electric field $\vec{E}$. In the general case, all four temperatures T_j are different and $\hat{\sigma}$ is very awkward. Let us consider three simple cases.

(a) $\vec{E}$ along $\langle 100\rangle$. In this case the four valleys are equivalent and the microwave mobility is

$$\hat{\mu} = \tfrac{1}{3}(2\hat{\mu}_t + \hat{\mu}_l) . \tag{A2}$$

For n-Ge, $\tau_t > \tau_l$ and $m_t \ll m_e$. Thus

$$2Z(\langle 100\rangle) \simeq \omega\tau_t . \tag{A3}$$

(b) $\vec{E}$ along $\langle 111\rangle$. Now there are two families of valleys. With evident notations,

$$\hat{\mu}(\langle 111\rangle) = \frac{n_1\hat{\mu}_{l1} + \frac{1}{3}n_2(8\hat{\mu}_{t2} + \hat{\mu}_{l2})}{3n_2 + n_1} , \tag{A4}$$

where n_1 and n_2 are, respectively, the numbers of electrons in the cold and hot valleys. If the intervalley transition time τ_{iv} is such that $\omega\tau_{iv} \gg 1$, the valley-density modulation is weak and $\hat{\sigma} \sim \hat{\mu}$; from Eq. (A4) one can see, with the above simplifications, $2Z\langle 111\rangle \sim \omega\tau_{t2}$.

(c) $\vec{E}$ along $\langle 110\rangle$. Now we have again two sets of hot and cold valleys:

$$\hat{\mu}(\langle 110\rangle) = \frac{n_2\hat{\mu}_{t2} + \frac{1}{3}n_1(\hat{\mu}_{t1} + 2\mu_{l1})}{n_1 + n_2}\, l . \tag{A5}$$

As in the preceding case, the electronic temperatures are not very different and again $2Z \sim \omega\tau_{t2}(\langle\epsilon\rangle)$, with poorer accuracy if $n_2 = n_1$ (20%).

APPENDIX B

We compare the mean power lost in electron–acoustical-phonon collisions to the mean power with optical phonons, ionization collisions, and interelectronic collisions.

1. Optical (and Intervalley) Phonons

The optical-phonon emission occurs for the energy tail of the distribution function, since the lattice temperature is very low $[N_q(\hbar\omega_0) \ll 1]$ and only electrons of sufficient energy can emit phonons. The general expression of the mean power lost is

$$\left\langle \frac{d\epsilon}{dt} \right\rangle_0 \sim E_0^2 \, \frac{\int_0^{q_M} q\,dq \int_{p_m}^{\infty} f_0(\epsilon + \hbar\omega_0)\, p\, dp}{\int_0^{\infty} f_0(\epsilon)\, p^2\, dp} . \tag{B1}$$

Clear derivations of (B1) are given in Conwell,[24] with the same notations for q_M, E_0, ω_0, etc. If the distribution function $f_0 \sim \exp[-(\epsilon/kTe)^{\delta}]$, Eq. (B1) yields approximately

$$\left\langle \frac{d\epsilon}{dt} \right\rangle_0 \sim E_0^2 \left(\frac{\hbar\omega_0}{kTe}\right)^{3-\delta} \frac{(kT_e)^{3/2}}{\Gamma(\frac{3}{2}\delta)} \exp\left[-\left(\frac{\hbar\omega_0}{kTe}\right)^{\delta}\right] . \tag{B2}$$

Now $\hbar\omega_0/k \sim 420\,^{\circ}\mathrm{K}$ (n-Ge). The critical electronic temperature, above which the optical phonon is important, strongly depends on δ. Now $\langle d\epsilon/dt\rangle_0$ is compared to $\langle d\epsilon/dt\rangle_a$, the mean power lost with acoustical phonons:

$$\left\langle \frac{d\epsilon}{dt} \right\rangle_a \sim E_1^2 (kT_e)^{3/2} \, \frac{\Gamma(3/\delta)}{\Gamma(\frac{3}{2}\delta)} . \tag{B3}$$

For $\delta = 1$, $\langle d\epsilon/dt\rangle_0 = \langle d\epsilon/dt\rangle_a$ at $T_e = 65\,^{\circ}\mathrm{K}$. With $\delta = 2.5$, the critical temperature becomes $\sim 300\,^{\circ}\mathrm{K}$. Thus, until the interelectronic processes intervene, the role of the optical phonon remains weak over the whole range of electric field 0–$30\ \mathrm{V\,cm^{-1}}$.

2. Ionization Collisions

The energy lost in one collision is $\simeq \epsilon_i$. Thus the mean power lost is of the order

$$\left\langle \frac{d\epsilon}{dt} \right\rangle_{i0} \simeq A_I(E)(N_D - N_A)\epsilon_i . \tag{B4}$$

Now for very hot electrons the problem is more complex, since the energy tail is modified by the ionization collisions. The comparison of (B4) and (B3) yields a theoretical law for A_I. If the acoustical phonon predominates, one can choose $A_I \sim A_I^0 \exp[-(-E_c/E)^2]$, the value of A_I^0 depending on the geometrical cross section and ϵ_i. A more rigorous analytical solution for A_I is now derived from the dependence $\sigma_i(\epsilon) \sim [(\epsilon - \epsilon_i)/\epsilon_i]\sigma_0$ (which is valid within $\epsilon_i < \epsilon < 2\epsilon_i$). Hence, if $\langle\epsilon\rangle < 2\epsilon_i$

$$\left\langle \frac{d\epsilon}{dE} \right\rangle_{i0} \simeq \frac{(2\epsilon_i)^{3/2}\sigma_0(N_D - N_A)}{\delta^2\Gamma(\frac{3}{2}\delta)\sqrt{m^*}} \left(\frac{kT_e}{\epsilon_i}\right)^{2\delta-5/2} \times\left[\delta + 3\left(\frac{kT_e}{\epsilon_i}\right)^{\delta-2}\right] \exp\left[-\left(\frac{\epsilon_i}{kT_e}\right)^{\delta}\right] . \tag{B5}$$

For $kT_e \simeq 0.7\ \epsilon_i$, $\delta = \frac{5}{2}$, the comparison of (B4) and (B5) with $N_D - N_A = 10^{15}\ \mathrm{cm^{-3}}$ yields $\langle d\epsilon/dt\rangle_{i0} = \langle d\epsilon/dt\rangle_a$. For $kT_e = 2\epsilon_i$ ($E \gg E_c$), $N_D - N_A = 10^{14}\ \mathrm{cm^{-3}}$ is sufficient to give $\langle d\epsilon/dt\rangle_{i0} \sim \langle d\epsilon/dt\rangle_a$, which perhaps explains the deviation of $A_I(E)$ above $E = 2E_c$ (Fig. 11). Then if $E > 30\ \mathrm{V\,cm^{-1}}$, the optical-phonon processes become of increasing importance and a new and complete derivation of the Boltzmann equation is needed with impact ionization and both optical- and acoustical-phonon processes.

3. Interelectronic Collisions

The mean power lost in interelectronic collisions is usually taken as

$$\left\langle \frac{d\epsilon}{dt} \right\rangle_{ee} = \frac{4\pi ne^4}{K_R^2} \left\langle \frac{1}{p} \right\rangle . \tag{B6}$$

The comparison of (B6) with (B3) within the zero-point limit gives a critical density n_e, where the interelectronic process may intervene $n_e \sim 10^{14}$ cm^{-3} for $\langle\epsilon\rangle \sim \epsilon_i$ [in fact, Eq. (B6) is deduced once the predominance of interelectronic process is assumed].

[1]S. Koenig, R. D. Brown, and W. Shillinger, Phys. Rev. 128, 4 (1962).
[2]A. Zylbersztejn, Phys. Rev. 127, 3 (1962).
[3]E. I. Abaulina-Zavaritskaya, Zh. Eksperim. i Teor. Fiz. 36, 1342 (1959) [Sov. Phys. JETP 9, 953 (1959)].
[4]E. I. Zavaritskaya, Fiz. Tverd. Tela. 6, 3545 (1964) [Sov. Phys. Solid State 6, 2839 (1965)].
[5]J. F. Le Hir, J. Phys. (Paris) 28, 805 (1967).
[6]V. A. Chuenkov, Fiz. Tek. Polup. 2, 353 (1968) [Sov. Phys. Semicond. 2, 292 (1968)].
[7]M. Lax, Phys. Rev. 119, 5 (1960).
[8]G. Ascarelli and S. Rodriguez, Phys. Rev. 129, 1321 (1961).
[9]D. R. Hamann and A. L. Mc Worther, Phys. Rev. 139, 1A (1964).
[10]I. Melngailis and A. G. Milnes, J. Appl. Phys. 33, 3 (1962).
[11]A. L. Mc Worther and R. H. Rediker, Proc. IRE 47, 1207 (1959).
[12]E. M. Conwell, Phys. Rev. 135, A814 (1964).
[13]A. Zylbersztejn and E. M. Conwell, Phys. Rev. Letters 11, 417 (1963).
[14]J. F. Palmier, Phys. Rev. Letters 25, 864 (1970).
[15]H. F. Budd and N. Perrin, Phys. Rev. (to be published).
[16]J. F. Palmier, Ph.D. thesis (Paris, 1972) (unpublished).
[17]J. C. Slater, *Microwave Electronics* (Van Nostrand, New York, 1960).
[18]B. Agdur and B. Ernander, J. Appl. Phys. 33, 2 (1962).
[19]A. Gibson, J. W. Granville, and E. G. S. Paige, J. Phys. Chem. Solids 19, 198 (1961).
[20]P. J. Price (unpublished); for a discussion of Eq. (7), see Ref. 1.
[21]H. F. Budd, Phys. Rev. 134, A1281 (1964).
[22]H. F. Budd, *Progress in the Physics of Semiconductors* (Dunod, Paris, 1964).
[23]C. Herring and E. Vogt, Phys. Rev. 101, 3 (1956).
[24]E. M. Conwell, Solid State Phys. Suppl. No. 9 (1967).
[25]R. Stratton, Proc. Roy. Soc. (London) A242, 355 (1957).
[26]C. Erginsoy, Phys. Rev. 79, 1013 (1950).
[27]H. Brooks, Phys. Rev. 83, 879 (1951).
[28]L. V. Keldysh, Zh. Eksperim. i Teor. Fiz. 48, 1692 (1965) [Sov. Phys. JETP 21, 1135 (1965)].
[29]A. Zylbersztejn, Phys. Rev. Letters 19, 838 (1967).
[30]S. Koenig, in *Proceedings of the International Conference on Solid State Physics, Brussels*, 1958 (Academic, New York, 1958), Vol. 1, p. 422.
[31]H. F. Budd, Phys. Rev. 127, 4 (1962).
[32]H. F. Budd, J. Phys. Soc. Japan 18, 142 (1963).
[33]W. Shockley, Solid-State Electron. 2, 1 (1961).
[34]L. V. Keldysh, Zh. Eksperim. i Teor. Fiz. 37, 713 (1959) [Sov. Phys. JETP 10, 509 (1960)].

PHYSICAL REVIEW B VOLUME 6, NUMBER 12 15 DECEMBER 1972

Changes in ac Conductivity of Silicon with Electron Irradiation at 0.5 K*

P. S. Gwozdz and J. S. Koehler
Department of Physics, University of Illinois, Urbana, Illinois 61801
(Received 6 July 1972)

Si was irradiated with 1.5-MeV electrons at 0.5 K. Changes in ac conductivity were dependent upon the dopant in the Si. No significant recovery of ac conductivity was observed with annealing up to 300 K. These results are consistent with previously published results at 1.6 K. These data support the suggestion that athermal migration of the Si interstitial occurs.

In a previous experiment[1] Si was irradiated at 5.0 and 1.6 K and changes in ac hopping conductivity were observed. This paper extends that work to 0.5 K.

A one-cycle pumped-He^3 cryostat was used in this experiment; the lowest temperature achieved was 0.3 K and the temperature during irradiation with 2×10^{10} e^-/cm^2 sec was 0.5 K. A carbon resistance thermometer was calibrated for each run against the vapor pressure of He^3. The University of Illinois Van de Graaff accelerator was used to provide 1.5-MeV electrons. The Si samples were wafers lapped to 400-μm thickness and then etched to nominally 3 cm$\times$2 cm$\times$150 μm. Gold circles 0.64 cm in diameter were evaporated on both sides of the wafers opposite each other and the electron beam was collimated to 0.7 cm in diameter so that only the sample capacitor (the two evaporated gold plates with the Si dielectric between them) was irradiated. The sample was surrounded by a copper shield at 1.6 K (pumped He^4) with aluminum-foil windows for the beam. Electrical contact was made to the gold plates via evaporated gold wires which were misaligned with respect to each other on the wafers in order to avoid stray capacitance. The wafers were glued with GE 7031 varnish to